Available online at www.sciencedirect.com
SCIENCE DIRECT®
ELSEVIER
International Journal of Solids and Structures 43 (2006) 713–726
INTERNATIONAL JOURNAL OF SOLIDS and STRUCTURES
www.elsevier.com/locate/ijsolstr

The onset and progression of damage in isotropic paper sheets

P. Isaksson *, P.A. Gradin, A. Kulachenko

Division of Solid Mechanics, Mid Sweden University, SE-851 70 Sundsvall, Sweden

Received 6 October 2004; received in revised form 11 April 2005
Available online 14 June 2005

Abstract

An experimental investigation is performed and analyzed in order to examine the onset and evolution of damage processes in thin isotropic paper sheets made of mechanical pulp. A microscopy technique has been used to estimate the relative fraction of bond and fibre breaks. It has been found that the active damage mechanism is bond failure, hence supporting the assumption of an isotropic scalar valued damage variable.

All experiments have been performed by simultaneous with the mechanical loading monitoring the acoustic emission activity. Three different experimental setups have been designed offering the possibility to analyze the influence of stress gradients, as well as different levels of the ratios between the in-plane normal stresses, on the onset of damage. It is concluded that stress gradients in the paper specimens have a large influence on the onset of damage. When stress gradients are present a non-local theory has to be used in the analysis. In this way compliance with an isotropic damage criterion is achieved. The characteristic length, determining the gradient sensitivity, has been found to be of the same order of magnitude as some average fibre length.

To study the evolution of the damage processes, wide and short specimens have been loaded in tension resulting in stable damage processes. With the assumptions made regarding the mechanical behavior of the paper material after onset of damage, the damage and the cumulative number of acoustic events curve correlates very well. The experimentally obtained data is used to determine material parameters in a proposed damage evolution law. It is found that the assumed damage evolution law can, for isotropic paper materials with bond rupture as the prevalent failure mechanism, be further simplified as only one specific material dependent damage evolution parameter has to be determined in experiments.

Keywords: Isotropic damage; Bond failure; Gradient sensitivity; Paper material

* Corresponding author. Tel.: +46 6014 8882; fax: +46 6014 8820.
E-mail address: per.isaksson@miun.se (P. Isaksson).

0020-7683/$ - see front matter © 2005 Elsevier Ltd. All rights reserved.
doi:10.1016/j.ijsolstr.2005.04.035

1. Introduction

Acoustic Emission (AE) monitoring is used in this investigation to detect the onset and evolution of damage processes in thin isotropic paper sheets. The detected emitted waves are a consequence of rapid release of elastic energy originating from micro failures (damage). A description of the method and its application to paper materials can be found in, among others, Gradin et al. (1997) or Yamauchi (2004).

In tensile experiments it has been observed that before the onset of acoustic emission, the stress–strain curve will deviate from linear behavior and upon unloading there will be a permanent deformation. One will, in addition to damage growth, also have another irreversible process commonly (but perhaps not correctly in this context) referred to as plasticity. However, plasticity processes occurs at a slower time scale than the fast release of elastic energy that originates from micro failures. Hence, it is generally anticipated that acoustic emission is not affected by plasticity processes (cf. Yamauchi, 2004).

Microscopic material failure in the paper during loading is treated in a "smeared out" sense using a concept of continuum damage mechanics, originally introduced by Kachanov (1958). If it is assumed that the degradation of the mechanical properties in isotropic paper sheets can be described by a single scalar parameter D, it can be shown that the thermodynamic damage driving force (often referred to as the damage energy release rate) and which is conjugate to the damage rate in the expression for the intrinsic energy dissipation, is related to the elastic energy density (amid others Hansen and Schreyer, 1994) and it is natural to assume that damage is onset at some critical value of this parameter.

In classic damage mechanics theory it is assumed that the damage driving force in a point is determined by the stress state in that point only. However, it has been claimed (cf. Pijaudier-Cabot and Bazant, 1987) that continuum damage is non-local in nature, meaning that a non-local model has to be introduced in the constitutive model. A review of non-local models can be found in Jirásek (1998), among others. The non-local model abandon the classical assumption that the damage driving force in a given point in the continuum is uniquely determined by the stress state in that point only as the model take into account interactions with the stress field in a neighborhood of that point. If there is no influence of the stress gradients in the vicinity of the point of onset of damage or, which is assumed to be the same thing: the onset of Acoustic Emission (AE), then one should observe the onset of AE for every stress state that touches the critical elastic strain energy density envelope, irrespective of the stress field in a vicinity of the point in question.

To dwell deeper into this matter, both uniaxial and biaxial experiments have been carried out on paper specimens cut from isotropic hand sheets with an area weight of 60 g/m^2, made of mechanical pulp. Tensile tests have been performed in two ways and in a standard laboratory environment, first on long and slender paper specimens and then on short and wide ones. In addition, a biaxial test has been designed that introduces stress gradients in circular paper specimens under controlled procedures in order to examine the influence of stress gradients on the onset of damage.

The short and wide specimens have also been used to study the damage evolution in the paper material because the geometry makes it possible to study also the post-peak behavior of the stress–strain curve since the damage processes in this case are stable in nature.

In all experiments, AE activity monitoring was performed simultaneous with the mechanical loading to determine the onset of damage and to follow the evolution of the damage processes. Finally, a microscopic study has been performed in order to reveal which fracture process (e.g., fibre/fibre bond break or fiber break) that is dominant during the degradation process.

2. Theory

Continuum damage mechanics is in its simplest form realized by introducing an isotropic scalar damage variable D, which is taking values in the range 0 (undamaged) to 1 (completely ruptured). In

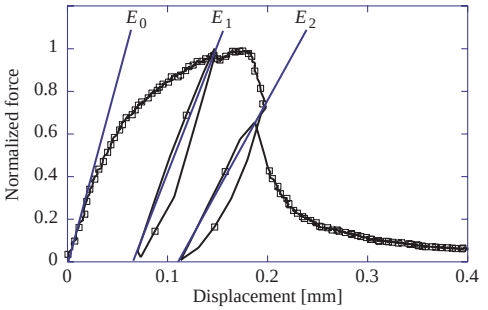

Fig. 1. Experimental illustration of material degradation by unloading and reloading.

theory, the variable D can be interpreted as a reduction of the load carrying area. Fig. 1 shows a typical force–displacement curve for the studied isotropic paper on a specimen with a high width/length ratio. Details regarding the paper material and the specimen geometry will be discussed later on. A few cycles of unloading and reloading have been made during the test in order to illustrate the material degradation. Denote the initial stiffness as E_0 and the two (degraded) stiffness on both sides of the peak-load as E_1 and E_2, Fig. 1. The ratios E_1/E_0 and E_2/E_0 are approximately 0.7 and 0.5. As the stiffness is decreasing, the result supports the assumption of material degradation.

To develop a constitutive model in which the effect of damage is included, one has to make some assumptions regarding in which way the damage will affect the mechanical properties. For example, one has to determine if the damage process will affect all material properties to the same extent (i.e., isotropic damage) or not. One also has to know (or make some assumption about) the number of separate damage mechanisms that becomes active during the loading process. However, as will be discussed later (Section 3.4), microscopic studies have revealed that the dominating damage mechanism in the examined isotropic paper sheets is *bond failure*, which supports the assumption of a scalar valued isotropic damage parameter.

An assumption of elastic energy equivalence is made (cf. Cordebois and Sidoroff, 1979; or Hansen and Schreyer, 1994) which means that the elastic energy density in a damaged material element is of the same form as that of a virgin material except that the actual stress tensor σ_{ij} is replaced by an effective stress tensor $\hat{\sigma}_{ij}$, i.e.,

$$\sigma_{ij} = (1 - D)\hat{\sigma}_{ij}. \tag{1}$$

Obviously, $\sigma_{ij} = \hat{\sigma}_{ij}$ for an undamaged material and $\sigma_{ij} \to 0$ at the moment of rupture.

If one damage scalar parameter D is sufficient to describe the influence of continuum damage in a point, the driving force for the damage evolution in that point would be the local damage energy release rate Y given by $Y = \partial\psi/\partial D$, where ψ is the elastic stress (complementary) energy density (cf. Hansen and Schreyer, 1994). Assuming that the paper material in its virgin state is linear elastic and that the damage is isotropic, then

$$Y = \frac{1 + \nu}{E(1 - D)^3}\left[\sigma_{ij}\sigma_{ij} - \frac{\nu}{1 + \nu}\sigma_{kk}\sigma_{ll}\right], \tag{2}$$

where E is the modulus of elasticity, ν is the Poisson's ratio and repeated index assumes summation.

For a local theory, this means that when Y reaches a critical value Y_c in a certain point, damage will be onset in that point. However, it has been reported (cf. Isaksson et al., 2004) that damage in paper materials is non-local in nature, meaning that not only does the value of Y in a certain point in the continuum affect the damage process, but also the stress fields in a neighborhood to that point. An intrinsic (internal) length,

or gradient sensitivity, determines this influence. Introducing a gradient sensitivity parameter is physically motivated by the microstructure of the paper material. Paper materials are considered as inhomogeneous solids containing many long fibres connected in a network. At any point those fibres apply non-local actions. It seems reasonable to assume that the elastic energy density in a particular point in a fibre is dependent upon the stress fields in the neighboring fibre network, or along the fibre itself.

If a non-local theory is applicable, a non-local damage driving force $\overline{Y}$ in a point may (cf. Lasry and Belytschko, 1988; Mühlhaus and Aifantis, 1991; or Peerlings et al., 1996) be obtained from the following truncated partial differential equation:

$$\overline{Y} = Y + c^2\nabla^2 Y, \tag{3}$$

where c is a gradient length parameter. The Laplacian operator is defined as $\nabla^2 = \sum_i \partial^2/\partial x_i^2$.

Peerlings et al. (1996) approximated equations of the class of the explicit formulation in Eq. (3) with an implicit gradient enhanced formulation resulting in an inhomogeneous elliptic equation that is suitable to incorporate in finite element analyses. Following Peerlings et al. a non-local elastic stress energy release rate $\overline{Y}$ was introduced in Isaksson et al. (2004),

$$\overline{Y} - \frac{1}{2} l^2 \nabla^2 \overline{Y} = Y, \tag{4}$$

where derivatives of order four and higher have been neglected. It is here assumed that $\overline{Y}$ admit at least Fréchet derivatives. It should be noted that Pijaudier-Cabot and Bazant (1987) proposed a similar expression for $\overline{Y}$ except that they used an approach based on a principle of strain equivalence. For further insight into the development of implicit gradient enhanced formulations the reader is referred to Peerlings et al. (1996) or Geers (1997), among others. The gradient sensitivity parameter l in Eq. (4) is a characteristic length that determines the volume that contributes significantly to the non-local damage energy release rate and must therefore be related to the scale of the microstructure in the material.

The solution of Eq. (4) requires additional boundary conditions. Following Lasry and Belytschko (1988) or Mühlhaus and Aifantis (1991) the natural Neumann type boundary condition of a vanishing gradient is used along the boundary Γ surrounding the entire problem domain,

$$n\nabla\overline{Y} = 0, \tag{5}$$

where n is the normal to the boundary Γ.

The (irreversible) damage evolution law is assumed as (for continuous damage),

$$D = 1 - \mathrm{e}^{-k(\overline{Y}/Y_c - 1)^m} \quad \text{for } \overline{Y} = H, \tag{6}$$

where k and m are arbitrary parameters determining the damage evolution which can be determined in experiments. The damage threshold H is the maximum value that $\overline{Y}$ has reached during the strengthening history (with the initial value Y_c), thus representing an isotropic damage hardening behavior. Eq. (6) was derived by observing, in acoustic emission experiments, that the damage increment $\mathrm{d}D$ seems to correlate to $(1-D)\mathrm{d}\overline{Y}$. The interested reader is advised to an article published elsewhere (Isaksson et al., 2004) for a more comprehensive discussion upon the development of Eq. (6).

3. Experiments

3.1. Onset of damage

It is understood that the influence of gradient sensitivity on the onset of damage in paper materials can be studied by performing experiments in which stress gradients are introduced under controlled procedures.

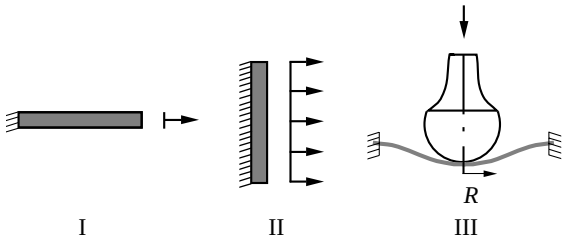

Fig. 2. Illustrations of load cases I–III.

In order to investigate the influence of stress gradients on the onset of damage, three basically different situations are considered. In the two first situations the stress fields are approximately homogenous in the specimens and, consequently, the stress gradients vanish. In addition, the third situation considers a situation in which stress gradients are introduced and makes it possible to analyze the non-local nature of the damage process.

The three situations are described below and illustrated in Fig. 2.

I. *Uniaxial stress tests.* Slender paper specimens with a low width/length ratio are loaded until onset of AE. In this case the resulting stress field is uniaxial and homogenous.
II. *Uniaxial strain tests.* Paper specimens with high width/length ratios are loaded until onset of AE. In this case, the resulting stress field is biaxial and homogenous.
III. *Biaxial tests with stress gradients.* This situation is accomplished by loading circular paper specimens (with their boundary held fixed) with semi-spherical contact bodies of varying radii until onset of AE. In this loading case the stress field is not homogenous and non-local theory has to be invoked in a numerical analysis to properly account for the stress gradients introduced. The stresses in all locations in the specimens are calculated by using a finite element code.

3.2. Damage evolution

The continued damage evolution can be studied if the damage process is stable (or semi-stable). In a stable damage process during a displacement controlled tensile test, the stress continuously decreases as the displacement is increased up to total separation resulting in two fracture surfaces. For paper materials, this behavior can only be obtained using a relatively short gauge length. If the gauge length is too long, lots of elastic energy will be stored in the paper specimen prior to peak-load to be released in an unstable manner at a post-peak load elongation.

To study the damage evolution, in wide and short paper specimens (II in Fig. 2), some means to determine the scalar damage variable D has to be developed. Consider a typical stress–strain curve for this type of specimen, Fig. 3(a). Needless to say, the curve is obtained in a tensile test under conditions of controlled displacement. It is assumed that the damage field, as well as the stress field, in the paper sheet is homogenous. This is of course only an approximation, especially after localization of damage. From experiments it is known at which strain ε_D onset of the AE, or damage, occurs. The idea is to fit some analytical expression for the stress versus strain to the whole uniaxial strain interval $0 \leqslant \varepsilon \leqslant \varepsilon_D$, following a concept outlined by Lemaitre and Chaboche (1994). By extrapolating this relation to higher strain values, one might get an idea of how the non-linear stress–strain relation would have been without any damage. The analytical expression adopted is

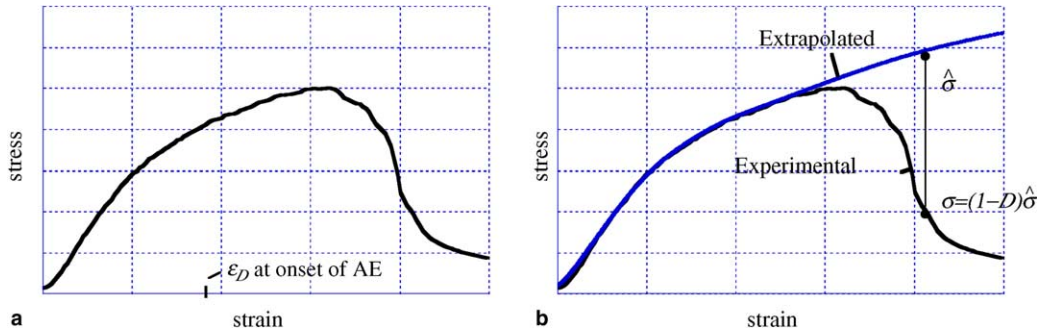

Fig. 3. (a) Typical stress–strain curve for a short and wide paper specimen. (b) Stress–strain curve with an extrapolated stress $\hat{\sigma}$.

$$\hat{\sigma} = \alpha\varepsilon + \beta\tanh(\gamma\varepsilon), \tag{7}$$

commonly attributed to Andersson and Berkyto (1951), where α, β and γ are arbitrary fitting variables. Since the damage parameter D represents a normalized loss of the load carrying area, the ratio $\sigma/\hat{\sigma}$ between the actual stress σ in the loading direction at a certain strain and the extrapolated stress $\hat{\sigma}$ at the same strain can be used to determine the damage parameter, Fig. 3(b).

Consider the damage evolution law assumed, i.e., Eq. (6), written on logarithmic form,

$$\ln[-\ln[1-D]] = \ln k + m\ln[\overline{Y}/Y_c - 1]. \tag{8}$$

The objective is to evaluate the damage variable D in experiments by using the relation $D = 1 - \sigma/\hat{\sigma}$ and to fit the damage constants k and m in the relation (8) in a least-square sense.

As the stress field in the paper specimen is assumed to be approximately homogenous in this experiment, the stress gradients vanish and the damage energy release rate is directly given by

$$\overline{Y} = \frac{\sigma^2(1-\nu^2)}{(1-D)^3 E}, \tag{9}$$

where the experimentally obtained stress in the loading direction is given by σ.

3.3. Test set-up and procedure

The tests were performed in a MTS servo hydraulic testing machine. During testing both the displacement and the load was monitored and recorded. A computer was used to control the load frame and also to record data during the testing. All tests were run to failure. In all experiments use was made of acoustic emission monitoring to detect the onset and evolution of the damage processes. The AE sensor, which is a piezoelectric resonance frequency sensor (resonance frequency 300 kHz) produced by the Acoustic Emission Technology company (AET), was positioned in the centre point of each specimen. The AE signals were recorded by using a system manufactured by Vallen Systeme GmbH.

Mechanical testing of paper must be carried out under humidity and temperature control in order to obtain reproducible results since paper is strongly influenced by moisture. The climate used was 23 °C and 50% RH that is in accordance with ISO 187. The samples were conditioned for at least 48 h in this environment prior to testing. All specimens were cut from isotropic hand sheets with a surface weight of 60 g/m^2 made of TMP with a Canadian Standard Freeness (CSF) of 90 ml. The Poissons' ratio of the material is $\nu = 0.32$. Standard methods were used to test structural properties. The standards used are ISO 534 for thickness and ISO 536 for basis weight.

Fig. 4. (a) Experiment I setup. The acoustic sensor is held fixed on the paper specimen by a hair clamp. (b) Experiment III setup without paper sample. The acoustic sensor, constrained in its vertical movement by a very weak spring, is clearly visible along with the semi-sphere used to load the paper. To fix the paper, it is placed on the inner cylindrical part, which is moved upwards and pressed against the steel ring at the top of the apparatus by means of a pneumatic pressure. (c) Experiment III setup with paper sample.

Three different specimen geometries have been used according to Section 3.3, namely:

I. *Uniaxial stress tests.* Specimens with a width of 10 mm and a gauge length of 80 mm.
II. *Uniaxial strain tests.* Specimens with a width of 80 mm and a gauge length of 10 mm.
III. *Biaxial tests with stress gradients.* Circular specimens with a radius of 35 mm. The semi-spherical contact bodies had radii R of 10, 20 and 35 mm.

The experiments are from now on denoted I–III, respectively.

A series of ten tests were carried out in each experiment I and II. For experiment III a series of five tests at each radius R of 10, 20 and 35 mm were carried out. In addition, in experiment III the paper specimens were impregnated with unpolar immersion oil, produced by the Merck company. The reason for adding the immersion oil is to decrease the influence of friction effects between the contacting body and the paper specimen during loading. Niskanen et al. (2001) reported that impregnation of paper with unpolar oils will not influence the strength properties of the paper sheet, at least not in the time range at which the experiments are performed.

Photos of the setups I and III are shown in Fig. 4. The setup of experiment II is similar to I as only the geometry of the specimen is different, and is not shown here.

3.4. Evaluation of damage mechanisms by microscopy

It is desirable to investigate if the damage mechanism producing AE in the paper is of a uniform type (bond failure) or whether both bond and fibre failures play an important role. For this reason notched slender samples (with a width of 15 mm, a gauge length of 100 mm and radius of the notches of 2.5 mm) were examined. In this experiment, specimens were made of 60 g/m^2 isotropic hand sheets of TMP with 2.5% by weight dyed fibres. It should be underlined that these hand sheets were made in the same way as the hand sheets used in the other experiments in this investigation, except that they also has a content of colored fibres. This does not affect any of the mechanical properties studied. The purpose of the notches is to force the fractured line to pass between the notches. In this way, the colored fibres after fracture could easily be compared to the fibres before fracture.

The challenge is to be able to observe the dyed fibres through the whole thickness of the paper specimen. To achieve this transparency, the paper was impregnated with the same immersion oil as used in III, and when the specimen was subjected to diffuse light, it was possible to observe all the dyed fibres through the thickness of the paper sheet, see Fig. 5.

As illustrated in Fig. 5(b), none of the colored fibres passing the fracture line have been broken. Then, by using diffuse light in a high-resolution scanner, it was possible to decide if the dyed fibres had ruptured during the paper fracture.

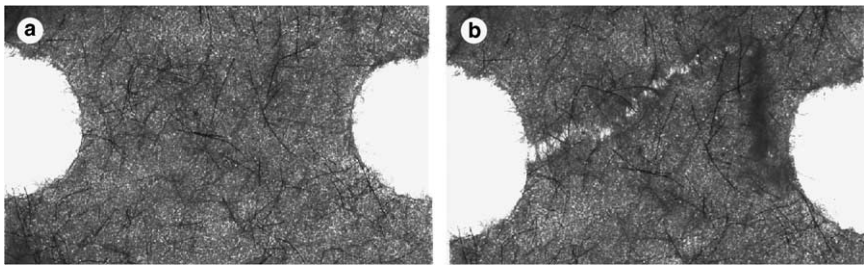

Fig. 5. (a) Notched sample with immersion oil and colored fibres before testing. (b) The same sample after the final rupture.

In the studied TMP based paper it was found that only 1 of 31 fibres crossing the rupture zone was broken during the final rupture of total 5 sheets. No fibre fractures were observed before the final fracture. The fibres that are passing the rupture zone (but are not broken) are pulled out of the fibre network on one of the sides of the fracture line. This pull out results in multiple bond breaks for each fibre. A conservative estimate is 10 broken bonds for each fibre. Based on the measurements, an estimation is made that at least 300 AE events are caused by broken bonds for each AE event caused by fibre rupture during the final fracture. Based on this observation it is concluded that the dominating damage mode is bond failure, which supports the assumption of an isotropic damage mechanism.

4. Analysis and results

4.1. Onset of damage: homogenous stress field

In experiment I and II the stress fields are approximately homogenous and the critical damage energy release rate Y_c at the onset of damage can be found analytically, i.e.,

$$Y_c = \sigma_{Ic}^2/E, \text{ in experiment I, and} \tag{10}$$

$$Y_c = \sigma_{IIc}^2(1-\nu^2)/E, \text{ in experiment II.} \tag{11}$$

Here σ_{Ic} and σ_{IIc} are the in-plane normal stresses in the loading direction at onset of AE in experiment I and II, respectively. In compliance with the isotropic damage criterion assumed, Y_c should be the same irrespective of the ratio between the in-plane normal stresses as long as the stress fields are homogenous. Thus, in theory, one expects to obtain the stress ratio $\sigma_{Ic}/\sigma_{IIc} = [1-\nu^2]^{1/2}$.

Fig. 6 shows typical results from the performed experiments I and II. Both force–displacement curves and curves showing the cumulative number of AE events are displayed.

The mean and standard deviation values after evaluation of all the ten performed experiments in each series I and II are $\sigma_{Ic}b \approx 7.3 \pm 0.3$ N/mm and $\sigma_{IIc}b \approx 7.7 \pm 0.7$ N/mm. The thickness of the paper is given by b.

It should here be noted that 20% of the experimental results have been excluded in both series I and II. The reason for that is that onset of AE in the excluded experiments were recorded at significantly lower loads than the average value (lower than 10% of the average onset stress values). The results from the excluded experiments are probably due to artifacts in the paper specimens (paper is an inhomogeneous material that naturally contains a population of flaws or other irregularities) or that the sensor somehow was not fixed properly to the specimens.

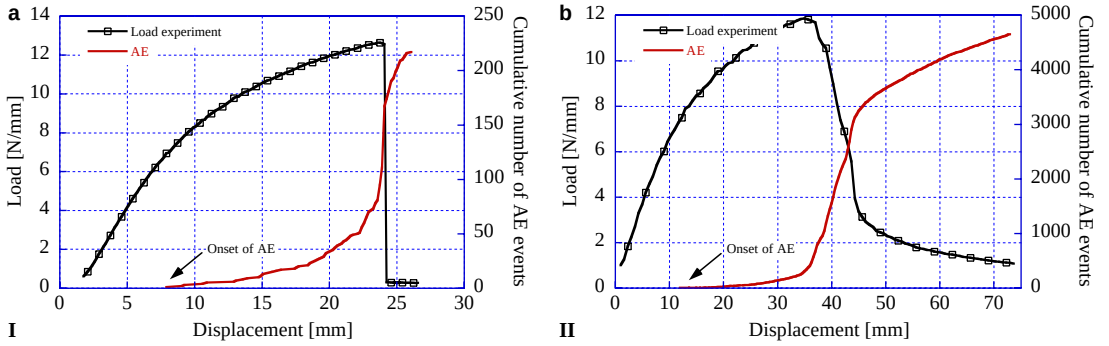

Fig. 6. Typical results from experiment I and II. The load is normalized with the width of the specimen in respective experiment (10 and 80 mm). One can, for these particular cases identify the stresses in the loading direction at onset for AE as $\sigma_{Ic}b \approx 7.1$ N/mm and $\sigma_{IIc}b \approx 7.3$ N/mm.

Using the mean stress values for onset of AE, the normal stress ratio $\sigma_{Ic}/\sigma_{IIc} = 0.95$ is in extremely good agreement with the theoretical value $[1 - \nu^2]^{1/2} = 0.95$. From the experimental result it can be concluded that, as long as the stress field is homogenous, the critical damage energy release rate Y_c (which is a material parameter) is independent of the ratio between in-plane normal stresses, which lends strong confidence to the analysis performed here and is in compliance with the isotropic damage criterion assumed. From Fig. 6(b) one can also observe that the non-linear material behavior, i.e., "plasticity", initiates at approximately half the displacement at which onset of AE occur, thus showing that plasticity in paper can exist without any acoustic emission.

4.2. Onset of damage: stress gradients

Finite element analyses have been performed in order to calculate the stress fields in the paper specimen at various levels of displacement, load and radius of the semi-sphere in experiment III. It is necessary to include numerical analysis since the stress field cannot be determined analytically. The non-linear stress–strain relationship (7) used for the examined paper material was obtained by using results from a uniaxial stress experiment.

The parametric mesh employed used 700 solid elements with rotational symmetry for the paper specimen, combined with 350 surface-to-surface contact elements for the contact between the semi-sphere and the paper specimen. For this part of the numerical analysis the commercial finite element code Ansys (2004) was used.

Fig. 7 shows typical experimentally obtained force–displacement curves as well as the corresponding calculated curves from the finite element analysis for the three different radii $R = 10$, 20, 35 mm of the semi-spherical contacting body. In Fig. 7 are also the cumulative number of AE events shown. The computed force–displacement curves agree very well with the experimentally obtained, which lends confidence to the finite element model.

After evaluation of all the five performed tests in each series could the mean value of the load P_c at which onset of AE occurred at each contact radius $R = 10$, 20, 35 mm be determined: $P_c(R = 10) \approx 0.89 \pm 0.02$ N, $P_c(R = 20) \approx 1.4 \pm 0.1$ N and $P_c(R = 35) \approx 2.2 \pm 0.1$ N. It should be mentioned that 20% of the experimental III results has been excluded from all series for the very same reasons as discussed in Section 4.1.

The specimens were then loaded, in the finite element analysis, until the mean loads P_c were reached. In this manner the stresses at all locations in the specimens at the load of onset of AE in the experiments could

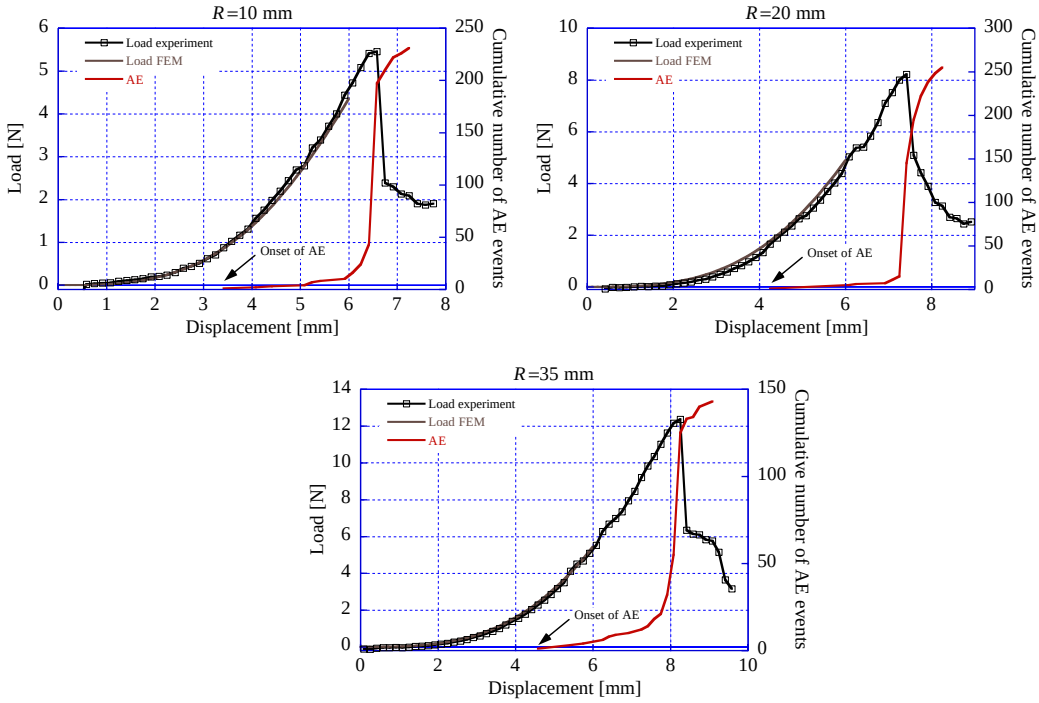

Fig. 7. Typical results obtained in experiment III with $R = 10$, 20, 35 mm. One can for these particular cases identify the load P_c at which onset of AE occur to $P_c(R = 10) \approx 0.9$ N, $P_c(R = 20) \approx 1.5$ N and $P_c(R = 35) \approx 2.2$ N. Also displayed are the corresponding force–displacement curves computed by FEM.

be calculated for respective load case. In the present situation the in-plane normal stresses σ_1 and σ_2 are equal in the centre of the circular specimen and approximately equal in the vicinity of that point. As the thickness of the paper sheet is extremely small, as compared to the radius of the sheet, the out-of-plane normal stress is assumed to vanish. When the stresses in all locations in the specimen at experiment III are computed, the local damage energy release rates Y at the load at which onset of AE occurred could be calculated. For the present loading situation one identifies $Y = 2\sigma^2(1 - \nu)/E$ and Eq. (4) is here written as

$$\overline{Y} - l^2\nabla^2\overline{Y}/2 = 2\sigma^2(1 - \nu)/E, \tag{12}$$

where σ is the biaxial stress.

The problem was then analyzed with a finite element model implemented in the Matlab code (2002) with the intention to study the effect of the present stress gradients. For further insight in the method the interested reader is advised to Isaksson et al. (2004).

In theory, at onset of AE $\overline{Y}_{\max} = Y_c = \sigma_{Ic}^2/E$, where $\overline{Y}_{\max}$ is the maximum damage energy release rate in the specimen and σ_{Ic} is the mean stress at which onset of AE occur in the uniaxial stress experiment. Needless to say, $\overline{Y}_{\max}$ appears at the location in the specimen where the stresses are highest, which is at the centre point or the point of contact with the "south-pole" of the semi-sphere.

For simplicity, Eq. (12) is written on a normalized form,

$$[\overline{Y}/Y_c] - l^2\nabla^2[\overline{Y}/Y_c]/2 = 2(1 - \nu)[\sigma^2/\sigma_{Ic}^2], \tag{13}$$

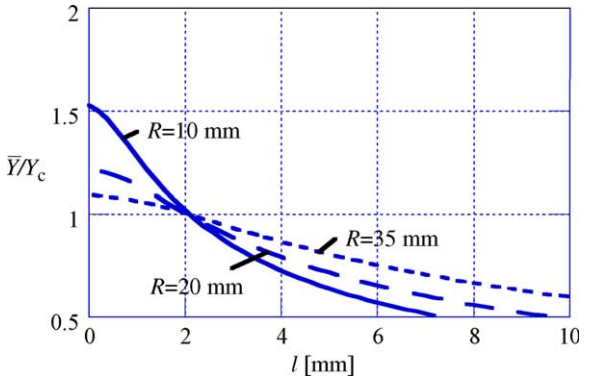

Fig. 8. Calculated maximum damage energy release rates $\overline{Y}/Y_c$ at various gradient sensitivity lengths l at the load of onset of AE at three load cases $R = 10$, 20, 35 mm. Note that $\overline{Y}/Y_c \approx 1$ when $l \approx 2$ mm for all the three load cases.

whereupon the influence of the thickness and the modulus of elasticity are cancelled. By solving Eq. (13) for each load case and with various characteristic lengths l one obtains the normalized maximum damage energy release rates $\overline{Y}/Y_c$, displayed in Fig. 8.

As Fig. 8 indicates, the influence of the stress gradients on the damage energy release rate $\overline{Y}$ is prevalent and illustrates the importance of using a non-local theory when studying the damage behavior in paper when the stress field is not homogenous. Using a local theory and thereby neglect the stress gradients in the specimen, the onset of AE occurs at $\overline{Y}/Y_c = 1.5$, 1.2, 1.1 for the load cases $R = 10$, 20, 35 mm, respectively.

However, introducing the stress gradients by using Eq. (13) in the analysis the result becomes different. When the characteristic length $l \approx 2$ mm then $\overline{Y}/Y_c \approx 1$ for all the three load cases. In this case the model predicts the very same loads for onset of AE that are obtained in all the experiments I, II and III, a result that is in compliance with the isotropic damage criterion assumed.

For a material consisting of a fibre network, an intuitive choice is to relate the characteristic length l to some average fibre length in the material, which for the present TMP based paper material is approximately 2 mm. Thus, the gradient sensitivity length found in the analysis turned out to be of the same order of magnitude as some average fibre length in the material. This is an appealing observation and is to some extent supported by previous investigations. Niskanen et al. (2001) concluded, in an experimental investigation on isotropic TMP based papers, that the width of a damage band developing when a paper specimen is loaded in tension until failure is governed by the mean fibre length.

4.3. Damage evolution

In experiment II the stress field is approximately homogenous and the damage process stable, and is therefore suitable for studying the continued damage evolution. Fig. 9 shows two typical stress–strain curves obtained in experiment II. For convenience, the measured experimental stress is normalized with its maximum value. The extrapolated theoretical stress curves $\hat{\sigma}(\varepsilon)$, according to relationship (7), are also drawn. Also displayed is the cumulative number of AE events as well as the evaluated damage variable D calculated by using the relation $D = 1 - \sigma/\hat{\sigma}$.

The cumulative number of AE events is normalized in the way so that 40% of the total number of cumulative events at the final fracture corresponds to a damage level of 40% in the material (i.e., $D = 0.4$). By studying the presented results in Fig. 9 one realizes that the detected AE indeed seems to indicate damage

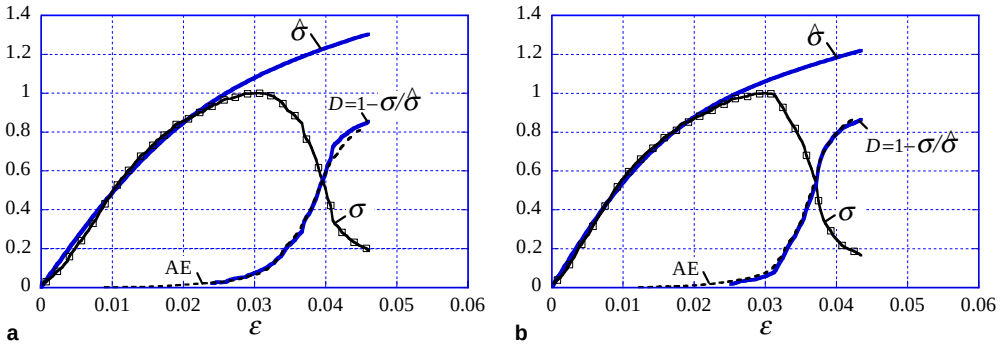

Fig. 9. Two typical experimental and theoretical stress–strain curves obtained in experiment II. Also displayed is the normalized cumulative number of AE events as well as the calculated homogenous damage variable D in the material as a function of the uniaxial strain ε.

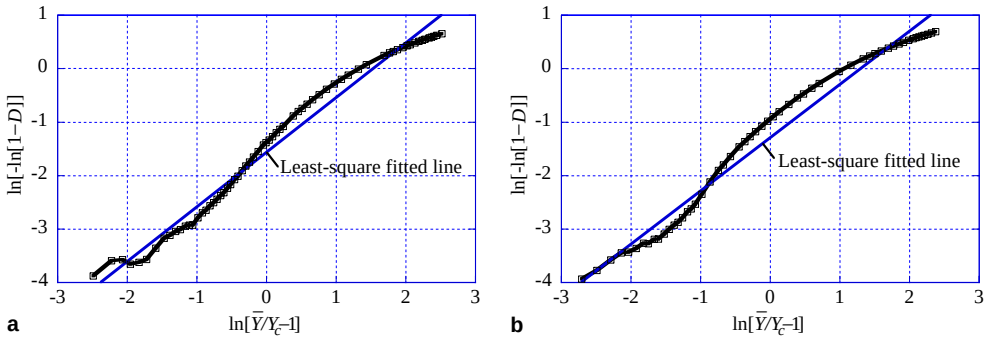

Fig. 10. Lines fitted in a least-square sense to Eq. (8), corresponding to the experiments in Fig. 9(a) and (b).

growth in the paper specimen, a conclusion that lends confidence to the analysis and methods used in this investigation.

Fig. 10 shows $\ln[-\ln[1-D]]$ as a function of $\ln k + m\ln[\overline{Y}/Y_c - 1]$, according to Eq. (8), for the corresponding experiments as shown in Fig. 9(a) and (b). Also displayed are least-square lines fitted to the experimentally obtained, and normalized, damage energy release rates $\overline{Y}/Y_c = (1-D)^{-3}[\sigma/\sigma_{IIc}]^2$.

The in the least-square sense determined parameter in Fig. 10 is $m = 1.02$ (a) and $m = 0.99$ (b). An assumption of $m = 1$ seems indeed appropriate for thin isotropic paper sheets.

It should be underlined that an assumption of $m = 1$ makes the damage evolution law in Eq. (6) particularly convenient, beside the numerical reasons, as only one specific damage evolution parameter (k) has to be determined in experiments. The logarithmic curves in Fig. 10 shows a nearly linear relationship. The conclusion is that the results presented in Figs. 9 and 10 implies that the rather simple damage evolution law assumed seems to describe the damage evolution in the paper material reasonable well, especially if one considers the simplifications made.

5. Conclusions

An investigation has been made to examine the onset and evolution of damage processes in thin isotropic paper sheets made of mechanical pulp. A microscopy technique has been used to estimate the relative

fraction of bond and fibre breaks. It has been found that the active damage mechanism is bond failure, which supports the assumption of an isotropic scalar valued damage variable. Three different experimental setups have been used in order to analyze the influence of the stress gradients, as well as various levels of the ratios between the in-plane normal stresses, on the onset of damage. To investigate the evolution of the damage processes, wide and short specimens have been loaded in tension resulting in stable damage processes. All experiments have been performed by simultaneous with the mechanical loading monitoring the acoustic emission activity in the paper specimens.

The following conclusions are made:

- Stress gradients in paper specimens have a large influence on the onset of damage.
- When stress gradients are present a non-local theory has to be used in the analysis. In this way compliance with an isotropic damage criterion is accomplished, regardless if the stress field is homogenous or not.
- It has been found that the characteristic length, determining the gradient sensitivity, is of the same order of magnitude as some average fibre length.
- With the assumptions made, it has been found that the damage growth and the cumulative number of acoustic events curve correlates well.
- It is found that the assumed damage evolution law can, for isotropic paper materials with bond rupture as the prevalent failure mechanism, be further simplified as only one specific material dependent damage evolution parameter has to be determined in experiments.

Acknowledgements

The fifth framework program of EU (QLK5-CT-2002-00772 AEP) is acknowledged for financing this work. The authors are grateful to Dr. Øyvind Gregersen and Dr. Per Nygård at PFI for assistance with the microscopy study.

References

Andersson, O., Berkyto, E., 1951. Some factors affecting the stress–strain characteristics of paper. Svensk Papperstidning 54, 437–444.

Ansys, 2004. Version 8.1. The Ansys Inc., Southpoint, USA.

Cordebois, J.P., Sidoroff, F., 1979. Endommagement anisotrope en élasticité et plasticité. J. Mécanique Appliquée (Numéro Spécial), 54–60.

Geers, M.G.D., 1997. Experimental analysis and computational modelling of damage and fracture. Ph.D. Thesis. Eindhoven University of Technology, The Netherlands.

Gradin, P., Nyström, S., Flink, P., Forsberg, S., Stollmaier, F., 1997. Acoustic emission monitoring of light-weight coated paper. J. Pulp Paper Sci. 23, 113–118.

Hansen, N.R., Schreyer, H.L., 1994. A thermodynamically consistent framework for theories of elastoplasticity coupled with damage. Int. J. Solids Struct. 31, 359–389.

Isaksson, P., Hägglund, R., Gradin, P., 2004. Continuum damage mechanics applied to paper. Int. J. Solids Struct. 41, 4731–4755.

Jirásek, M., 1998. Nonlocal models for damage and fracture: comparison of approaches. Int. J. Solids Struct. 35, 4133–4145.

Kachanov, L.M., 1958. Time of the rupture process under creep condition. Izv. Akad. Nauk SSSR, Otd. Tekhn. Nauk 26–31 (in russian).

Lasry, D., Belytschko, T., 1988. Localization limiters in transient problems. Int. J. Solids Struct. 24, 581–597.

Lemaitre, J., Chaboche, J.L., 1994. Mechanics of Solid Materials. Cambridge University Press, Cambridge, UK.

Matlab, 2002. Version 6.5. The MathWorks Inc., Natick, MA, USA.

Mühlhaus, H.-B., Aifantis, E.C., 1991. A variational principle for gradient plasticity. Int. J. Solids Struct. 28, 845–857.

Niskanen, K., Kettunen, H., Yu Y., 2001. Damage width: a measure of the size of fracture process zone. In: 12th Fundamental Research Symposium, Oxford, UK.

Peerlings, R.H.J., de Borst, R., Brekelmans, W.A.M., de Vree, J.H.P., 1996. Gradient enhanced damage for quasi-brittle materials. Int. J. Numer. Methods Eng. 39, 3391–3403.
Pijaudier-Cabot, G., Bazant, Z.P., 1987. Nonlocal damage theory. J. Eng. Mech. 113, 1512–1533.
Yamauchi, T., 2004. Effect of notches on micro failures during tensile straining of paper. Jpn. Tappi J. 58, 105–112.